


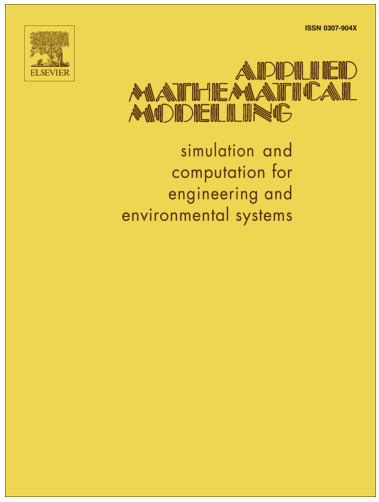


# Finite Volume Solutions for Electromagnetic Induction Processing

G. Djambazov, V. Bojarevics, K. Pericleous, N. Croft

PII: S0307-904X(15)00260-7
DOI: http://dx.doi.org/10.1016/j.apm.2015.03.059
Reference: APM 10553

To appear in: *Appl. Math. Modelling*

Received Date: 5 November 2014
Revised Date: 10 March 2015
Accepted Date: 16 March 2015

Please cite this article as: G. Djambazov, V. Bojarevics, K. Pericleous, N. Croft, Finite Volume Solutions for Electromagnetic Induction Processing, *Appl. Math. Modelling* (2015), doi: http://dx.doi.org/10.1016/j.apm.2015.03.059

# Finite Volume Solutions for Electromagnetic Induction Processing

G. Djambazov[a,*], V. Bojarevics[a], K. Pericleous[a], N. Croft[b]

[a] *Centre for Numerical Modelling and Process Analysis, University of Greenwich, UK*

[b] *College of Engineering, Swansea University, UK*

**Abstract**

A new method is presented for numerically solving the equations of electromagnetic induction in conducting materials using native, primary variables and not a magnetic vector potential. Solving for the components of the electric field allows the meshed domain to cover only the processed material rather than extend further out in space. Together with the finite volume discretisation this makes possible the seamless coupling of the electromagnetic solver within a multi-physics simulation framework. After validation for cases with known results, a 3-dimensional industrial application example of induction heating shows the suitability of the method for practical engineering calculations.

*Keywords:* electromagnetic field; induction heating; induction stirring; numerical solution of partial differential equations; pseudo-steady state; integral boundary condition; finite volume discretisation

## 1. Introduction

Induction heating and stirring is often used in the processing of conductive materials: melting of metals and alloys, controlling the temperature and stirring of liquid silicon, etc. Magnetic fields are also used to melt levitated samples for precise measurements of material properties. For chemically reactive alloys the magnetic field can help contain the melt in 'semi-levitation' or 'cold crucible' induction furnaces.

Computer modelling of those processes can be very useful for their optimisation. The

*Corresponding author
*Tel:* +442083319589
*Email address:* G.Djambazov@gre.ac.uk (G. Djambazov)

process usually involves several intertwined physical phenomena such as electromagnetic induction, heat transfer, phase change, elasto-plasticity, fluid flow with free surface, and magnetohydrodynamics.

An efficient way to capture the true interactions among all those phenomena can be the simulation by a single computer program [1] where the values of the solved variables are advanced simultaneously at each iteration and at each time step of the solution process. Some authors [2] also include thermo-mechanical (stress analysis) computations at each step of the algorithm for cases where the deformation of the material affects the electromagnetic field.

The electromagnetic fields involved in induction metal processing are three dimensional, and eddy currents are induced in the conducting objects. Their calculation has been addressed in various ways, with or without magnetic potentials, in finite element (FEM) and other formulations [4, 5, 6, 7]. Combining FEM and boundary element methods helps reduce the size of the meshed computational domain and, hence, the computational time [8]. This work does not attempt to include a more comprehensive review of the numerous formulations, algorithms and software implementations for modelling 3D electromagnetic phenomena.

In this work the finite volume method is used to discretise and solve the governing equations of electromagnetic induction. Such a formulation is compatible with the solution procedures for the other variables in a a thermo-fluid computational model. The resulting computer code readily fits into the PHYSICA framework [3]. It can also be used in combination with other finite volume PDE codes.

The algorithm described below is formulated in primary variables for the electric and the magnetic field and does not involve a magnetic vector potential. This presents an alternative to the potential formulation and allows a more 'natural' representation of the governing equations and of the boundary conditions on the conductor surfaces.

The implementation of the new method described here was added to a multi-physics computational environment [3] but the method itself is generic and can be attached to other partial differential equation (PDE) solvers.

The paper is organised as follows: first, the governing equations of electromagnetic induction are presented, then special attention is paid to the source term linearisation in the quasi-steady case. Various aspects of the boundary treatment are considered, and finally validation and sample results illustrate the applicability of the method.

## 2. Equations

Maxwell's equations in differential form describe the local relationship between the variables of the electromagnetic field. In the case of non-magnetic materials (non-ferrous metals or steel in a certain temperature range) the magnetic permeability $\mu$ may be assumed constant throughout the spatial domain of interest. On the other hand, in sufficiently conducting materials (including molten metals) there are no localised electric charges, and Maxwell's equations can be simplified to form the basis of the theory of electromagnetism [9]:

$$\operatorname{div} \mathbf{B} = 0 \tag{1}$$

$$\operatorname{curl} \mathbf{E} = -\partial \mathbf{B}/\partial t \tag{2}$$

$$\operatorname{curl} \mathbf{B} = \mu \mathbf{J} \tag{3}$$

$$\operatorname{div} \mathbf{E} = 0 \tag{4}$$

where $\mathbf{B}$ is the magnetic induction, $\mathbf{E}$ is the electric field intensity, $t$ is time, and $\mathbf{J}$ is the electric current density. Ohm's law provides an algebraic relation between $\mathbf{J}$ and $\mathbf{E}$, and for isotropic electrical conductivity $\sigma$ it can be written as $\mathbf{J} = \sigma \mathbf{E}$.

Assuming that $\mathbf{B}$ is sufficiently continuous so that its temporal and spatial derivatives may be swapped, taking the curl of (2), after substitution only one variable is left:

$$\operatorname{curl} (\operatorname{curl} \mathbf{E}) = -\mu \partial (\sigma \mathbf{E})/\partial t. \tag{5}$$

The electrical conductivity $\sigma$ depends on the temperature which changes with time. However, on the time scale of the electromagnetic processes, $\sigma$ may be assumed constant in time. Then, using the mathematical identity $\operatorname{curl} (\operatorname{curl} \mathbf{E}) = \operatorname{grad}(\operatorname{div} \mathbf{E}) - \nabla^2 \mathbf{E}$ and (4), equation (5) may be simplified into:

$$\nabla^2 \mathbf{E} = \mu \sigma \frac{\partial \mathbf{E}}{\partial t}. \tag{6}$$

The transient term and the diffusion term of the general conservation equation usually solved by Computational Fluid Dynamics (CFD) codes can easily be recognised in the above equation (6). So CFD codes may be used *directly* for transient simulations of electromagnetic phenomena just by switching off the convection term and providing the necessary boundary conditions.

In induction melting only alternating currents are used with typical frequencies in the range 1 to 10 kHz. The time scale of the electromagnetic phenomena is at least 50 times smaller then the time scale of the fluid phenomena. Consequently, the modelling of the fluid flow in the process requires the pseudo-steady solutions of the electric and the magnetic fields rather than their time-dependent behaviour.

Assuming that a periodic solution exists with a circular frequency $\omega$: $\mathbf{E} = \mathbf{E}_R \cos\omega t + \mathbf{E}_I \sin\omega t$, and substituting into (6), the following system results:

$$\nabla^2 \mathbf{E}_R = \mu\sigma\omega \mathbf{E}_I \tag{7}$$

$$\nabla^2 \mathbf{E}_I = -\mu\sigma\omega \mathbf{E}_R. \tag{8}$$

This system consists of six scalar equations for six unknown functions. The transient terms have disappeared and have been replaced by source terms. The magnitude of these source terms is substantial and they need to be linearised with respect to the unknown variables in order to achieve convergence within the CFD code; this is discussed in the next section.

From the solved values of $\mathbf{E}_R$ and $\mathbf{E}_I$ the components of the magnetic field $\mathbf{B}$ can be recovered according to (2) as

$$\mathbf{B}_R = -\frac{1}{\omega}\mathrm{curl}\,\mathbf{E}_I \tag{9}$$

$$\mathbf{B}_I = \frac{1}{\omega}\mathrm{curl}\,\mathbf{E}_R \tag{10}$$

with the curl operators evaluated numerically from the partial spatial derivatives of $\mathbf{E}$.

The **charge conservation** constraint (4) results in two more equations for the same variables: $\mathrm{div}\,\mathbf{E}_R = 0$ and $\mathrm{div}\,\mathbf{E}_I = 0$. One way of insuring non-divergence of the electric field vectors is by solving separately for their irrotational part ($-\nabla\varphi_{R,I}$) and rotational

part ($\mathbf{E}'_{R,I}$), the final solution being the sum of the two fields:

$$\mathbf{E}_R = \mathbf{E}'_R - \nabla\varphi_R \tag{11}$$

$$\mathbf{E}_I = \mathbf{E}'_I - \nabla\varphi_I. \tag{12}$$

The equations for the two scalar electric potentials $\varphi_R$ and $\varphi_I$ that are obtained from (11), (12) and (4)

$$\operatorname{div}(\nabla\varphi_{R,I}) = \nabla^2\varphi_{R,I} = \operatorname{div}\mathbf{E}'_{R,I} \tag{13}$$

can easily be solved in the same finite volume framework.

When (11) and (12) are substituted into (7) and (8) additional source terms appear and the equations for the rotational components become

$$\nabla^2\mathbf{E}'_R = \mu\sigma\omega\mathbf{E}'_I + \nabla^2(\nabla\varphi_R) - \mu\sigma\omega\nabla\varphi_I \tag{14}$$

$$\nabla^2\mathbf{E}'_I = -\mu\sigma\omega\mathbf{E}'_R + \nabla^2(\nabla\varphi_I) + \mu\sigma\omega\nabla\varphi_R. \tag{15}$$

Hence, the PDE system to solve will have eight equations (14, 15 and 13) with the eight unknowns being all three components of $\mathbf{E}'_R$ and $\mathbf{E}'_I$ plus $\varphi_R$ and $\varphi_I$. These are second order diffusion type equations where the right-hand side (RHS) of each one depends on unknowns 'belonging' to other equations from the system. An iterative approach to the numerical solution of the system is followed, i.e. the RHS is calculated from the values of the unknowns at the previous iteration. For better stability and convergence of the algorithm, partial linearisation of the RHS is done which transfers part of the RHS to the diagonal of the system matrix (solved at each iteration) and which is discussed in the following section.

### *2.1. Force and heat*

The purpose of treating a metal charge or a conducting liquid (e.g. molten silicon) with electromagnetic induction is to add heat and to stir the melt, so it is essential to accurately predict the forces acting and the heat released in the liquid material. In a unit of conducting volume the electromagnetically generated instantaneous Lorentz force $\mathbf{F}$ and Joule heat $Q$ are [9]

$$\mathbf{F} = \mathbf{J} \times \mathbf{B} \tag{16}$$

$$Q = \mathbf{J} \cdot \mathbf{E} = \sigma E^2. \tag{17}$$

Time-averaging of these sinusoidal quantities over one period yields the mean (quasi-steady) values

$$\mathbf{F}_{mean} = 0.5\ (\mathbf{J}_R \times \mathbf{B}_R + \mathbf{J}_I \times \mathbf{B}_I) \tag{18}$$

$$Q_{mean} = 0.5\ \sigma\ (\mathbf{E}_R^2 + \mathbf{E}_I^2). \tag{19}$$

*2.2. Useful particular cases*

The number of unknown variables can be reduced in **two-dimensional** models. Let us assume that the magnetic induction $\mathbf{B}$ has only one component in the $z$-direction $B_z = B$, and the other two components are zero. Then from equations (1), (2), and (3) we can obtain:

$$\frac{\partial B}{\partial z} = \frac{\partial E_x}{\partial z} = \frac{\partial E_y}{\partial z} = E_z = 0 \tag{20}$$

$$\frac{\partial E_y}{\partial x} - \frac{\partial E_x}{\partial y} = -\frac{\partial B}{\partial t} \tag{21}$$

$$\mu\sigma E_x = \frac{\partial B}{\partial y},\ \mu\sigma E_y = -\frac{\partial B}{\partial x} \tag{22}$$

Note that (4) is automatically satisfied when (22) is true. Also, in non-conducting areas ($\sigma = 0$), $\partial B/\partial x = \partial B/\partial y = 0$ which means

$$B = \text{const}\,. \tag{23}$$

For regions with $\sigma = \text{const}$ a single time-dependent equation for the magnetic induction may be obtained by further differentiating (22) and substituting into (21):

$$\frac{\partial^2 B}{\partial x^2} + \frac{\partial^2 B}{\partial y^2} = \mu\sigma\frac{\partial B}{\partial t} \tag{24}$$

In the quasi-steady case a convenient set of two differential equations for the magnetic induction variables results which is a two-dimensional scalar version of (7) and (8):

$$B = B_R \cos\omega t + B_I \sin\omega t \tag{25}$$

$$\frac{\partial^2 B_R}{\partial x^2} + \frac{\partial^2 B_R}{\partial y^2} = \mu\sigma\omega B_I \tag{26}$$

$$\frac{\partial^2 B_I}{\partial x^2} + \frac{\partial^2 B_I}{\partial y^2} = -\mu\sigma\omega B_R. \tag{27}$$

Further simplification is possible in the **one-dimensional** case which can be useful for a surface parallel to the magnetic field vector lines. In (22) if it is assumed that $E_x = 0$, it

follows that $\partial B/\partial y = 0$, and (26) and (27) are reduced to ordinary differential equations along $x$. It can be verified by substitution that their solution will be

$$B_R = B_0 \exp(-\frac{x}{\delta}) \cos \frac{x}{\delta} \ , \quad B_I = B_0 \exp(-\frac{x}{\delta}) \sin \frac{x}{\delta} \tag{28}$$

where $\delta$ is defined by the equation $\mu\sigma\omega\delta^2 = 2$, and $B_0$ is the magnetic induction on the surface at the beginning of each cycle. Then from (22) we obtain

$$E_R = \frac{\omega\delta}{2}(B_R + B_I) \ , \quad E_I = \frac{\omega\delta}{2}(B_I - B_R). \tag{29}$$

One-dimensional approximation is appropriate for analysis of higher-frequency cases (with thinner electromagnetic skin depth $\delta$) and where the curvature of the surface is not great with the magnetic field lines parallel (or almost parallel) to it. Two-dimensional computation can be applied to non-axisymmetric middle cross-sections of longer billets or crucibles where the magnetic field lines become parallel to the treated surfaces. The above particular cases are also very useful for validating the general, 3-dimensional implementations as this can be seen in section 5.

## 3. Source terms linearisation

The general conservation equation solved by most CFD codes is in the form

$$\frac{\partial(\rho\phi)}{\partial t} + \mathrm{div}\,(\rho\mathbf{u}\phi) = \mathrm{div}\,(\Gamma_\phi\,\mathrm{grad}\phi) + S_\phi. \tag{30}$$

where $\rho$ is the fluid density, $\mathbf{u}$ is the fluid velocity, $\Gamma_\phi$ is the diffusion coefficient, $\phi$ is the unknown conserved variable, and $S_\phi$ is the source term. To achieve convergence of the iterative solution process in many cases it is necessary to represent the source term in the form

$$S_\phi = S_C - S_P\phi \tag{31}$$

with $S_P > 0$. This technique is called linearisation of the source term, and it often represents the physical dependence of the source term on its variable [10].

Consider the pair of equations (26) and (27); the result will apply also to the three components of the vector equations (7) and (8). These equations are particular cases of

the general conservation equation (30) where the transient term and the convection term on the left-hand side are set to zero and the diffusion coefficient is $\Gamma_\phi = 1$.

Examining the source terms, it can be seen that each of the unknown variables, $B_R$ and $B_I$, appears in the source term of the other variable's equation. Also, each variable may have its own sources due to the boundary conditions. Assume that each variable's own sources can be represented in the form (31). The discretised finite volume forms of the complete equations (26) and (27) will then be:

$$\sum_{f=1}^{n} A_f \frac{B_{R,f} - B_R}{d_f} + c_R - p_R B_R - q B_I = 0 \tag{32}$$

$$\sum_{f=1}^{n} A_f \frac{B_{I,f} - B_I}{d_f} + c_I - p_I B_I + q B_R = 0. \tag{33}$$

Here the summation is done over all the $n$ faces ($f$) bounding a given cell in the mesh, $A_f$ are the face areas, $B_{R,f}$ and $B_{I,f}$ are the values of the variables in the neighbouring cells across $f$, $d_f$ are the distances between the neighbouring cell centres, $q = \mu\sigma\omega V$ where $V$ is the cell volume; $c_R = (S_C)_{B_R} V$, $p_R = (S_P)_{B_R} V$, $c_I = (S_C)_{B_I} V$, and $p_I = (S_P)_{B_I} V$ are the respective linearised sources.

Equation (32) may be rearranged to form an expression for $B_R$. This expression can be used to remove $B_R$ from equation (33). Likewise (33) can be used to enable the removal of $B_I$ from (32). If the sums are split, denoting

$$\Sigma_R = \sum_{f=1}^{n} A_f \frac{B_{R,f}}{d_f}\,,\ \Sigma_I = \sum_{f=1}^{n} A_f \frac{B_{I,f}}{d_f}\,,\ \Sigma_0 = \sum_{f=1}^{n} \frac{A_f}{d_f}\,,$$

the discretised finite volume equations (32) and (33) can be written in the form:

$$\sum_{f=1}^{n} A_f \frac{B_{R,f} - B_R}{d_f} + \left(c_R - q\frac{\Sigma_I + c_I}{\Sigma_0 + p_I}\right) - \left(p_R + \frac{q^2}{\Sigma_0 + p_I}\right) B_R = 0 \tag{34}$$

$$\sum_{f=1}^{n} A_f \frac{B_{I,f} - B_I}{d_f} + \left(c_I + q\frac{\Sigma_R + c_R}{\Sigma_0 + p_R}\right) - \left(p_I + \frac{q^2}{\Sigma_0 + p_R}\right) B_I = 0. \tag{35}$$

The terms $\Sigma_I$ (in the $B_R$-equation) and $\Sigma_R$ (in the $B_I$-equation) each contain the other unknown variable. In the implementation, those values are taken from the previous iteration of the non-linear iteration loop. This means the linearisation of the source terms shown above is only partial but it helps transfer part of the magnitude of the source term onto the system matrix diagonal which makes the iterative solution of the linear system more stable. This form of the linearised source expressions is not ideal because one of the

equations still contains a negative coefficient in front of neighbouring values of the other variable. However, with a relaxation factor in the range 0.75 to 0.95, converged solutions have been obtained for most sets of boundary conditions.

## 4. Boundary conditions

Boundary conditions may be specified on the surface of the conducting objects. In this way the computational domain only covers the bodies with induced currents, and the action of the external driving coil is taken into account via Biot-Savart integration for the points on the surface. Symmetry may be used to reduce the size of the computational domain. In most cases that is azimuthal symmetry, and for vector quantities boundary expressions are also presented in this section.

### *4.1. Surface boundaries*

Faraday's equation(2) and the condition that there is no normal current through the surface provide the necessary boundary conditions.

#### *4.1.1. Induction condition*

In the quasi-steady case (25) Faraday's law of electromagnetic induction is represented by two vector equations:

$$\operatorname{curl}\mathbf{E}_R = -\omega\mathbf{B}_I\,, \quad \operatorname{curl}\mathbf{E}_I = \omega\mathbf{B}_R. \tag{36}$$

The two vectors of the magnetic induction $\mathbf{B}_R$ and $\mathbf{B}_I$ can be evaluated separately using the Biot-Savart formula (43) with the corresponding current density fields $\mathbf{J}_R = \sigma\mathbf{E}_R$ and $\mathbf{J}_I = \sigma\mathbf{E}_I$.

A local coordinate system is considered $(n, a, b)$ with an origin in the middle of a given cell face on the surface. Axis $n$ is defined by the outward normal vector to the face, axis $a$ has the direction of the vector defined by the first and the second corner points of the face, and axis $b$ is in the direction of the cross product $\mathbf{n} \times \mathbf{a}$ of the first two unit vectors. After expanding $\operatorname{curl}\mathbf{E}_R$ and $\operatorname{curl}\mathbf{E}_I$ in the local coordinate frame the induction boundary

condition (36) becomes:

$$\frac{\partial E_{nR}}{\partial b} - \frac{\partial E_{bR}}{\partial n} = -\omega B_{aI} \quad , \quad \frac{\partial E_{nI}}{\partial b} - \frac{\partial E_{bI}}{\partial n} = \omega B_{aR} \tag{37}$$

$$\frac{\partial E_{aR}}{\partial n} - \frac{\partial E_{nR}}{\partial a} = -\omega B_{bI} \quad , \quad \frac{\partial E_{aI}}{\partial n} - \frac{\partial E_{nI}}{\partial a} = \omega B_{bR}. \tag{38}$$

The components of **J** and **E** normal to the surface of the conducting bodies are zero. However, the quantities $E_{nR}$, and $E_{nI}$ are equal to zero only for the given cell face on the surface. (If the surface is not flat, the $n$-components of the neighbouring faces are nonzero with respect to the local coordinates.) This means that their derivatives with respect to $a$ and $b$ are not zero and have to be evaluated. This may be done in the following way. Let $r_a$ is the curvature radius of the surface in the plane $(a, n)$. In the vicinity of the observation point on the surface the intersection of plane $(a, n)$ with the surface is a circular arc. Let $\alpha$ be the central angle sweeping that arc. Then the projection onto axis $n$ of the tangential vector of magnitude $E_a$ turning along the arc will be $E_n = -E_a \sin\alpha$. Differentiating this with respect to $a$, bearing in mind that $a = r_a\alpha$, the equation $\partial E_n/\partial a = -(E_a/r_a)\cos\alpha$ is obtained which for the location of interest, $\alpha = 0$, gives

$$\frac{\partial E_n}{\partial a} = -\frac{E_a}{r_a} \tag{39}$$

$$\frac{\partial E_n}{\partial b} = -\frac{E_b}{r_b}. \tag{40}$$

The second equation (40) can be derived for the plane $(b, n)$ in exactly the same way as (39); then these equations can be applied to the $R$ and $I$ parts in (37) and (38) in order to obtain expressions for the normal derivatives of the tangential components:

$$\frac{\partial E_{bR}}{\partial n} = \omega B_{aI} - \frac{E_{bR}}{r_b} \quad , \quad \frac{\partial E_{bI}}{\partial n} = -\omega B_{aR} - \frac{E_{bI}}{r_b} \tag{41}$$

$$\frac{\partial E_{aR}}{\partial n} = -\omega B_{bI} - \frac{E_{aR}}{r_a} \quad , \quad \frac{\partial E_{aI}}{\partial n} = \omega B_{bR} - \frac{E_{aI}}{r_a}. \tag{42}$$

It can be seen that the above boundary sources are in a linearised form (31). The only difficulty is that they are in *local* coordinates, and the solved variables are *global* components of the field vectors. This means that it may not be possible to take advantage of the linearisation. This should not be a problem if the surface curvature is not to high. A backward transformation is done from local to global coordinates to determine the actual fluxes of the $x$, $y$, and $z$ components of the solved variables. Usually the Biot-Savart evaluation of the magnetic induction will be implemented in global coordinates, then the forward transformation will provide the necessary local components of $\mathbf{B}_R$ and $\mathbf{B}_I$.

*4.1.2. The singular integral of Biot-Savart*

Given the electric current density ($\mathbf{J}_R$, $\mathbf{J}_I$) within the time-harmonic (pseudo-steady) approximation, the corresponding induced magnetic field can be calculated as

$$\begin{aligned} \mathbf{B}_{R,I} &= \frac{\mu}{4\pi} \int\limits_{space} \frac{\mathbf{J}_{R,I} \times \mathbf{r}}{r^3} dV \\ \mathbf{r} &= \mathbf{r}_{observation} - \mathbf{r}_{source} \end{aligned} \tag{43}$$

where the volume integral is taken over all space, i.e. all conducting bodies including the excitation coil. On the surface where it is needed for the boundary conditions the integral is singular as $r$ tends to zero.

On a cell-centred mesh, like the one PHYSICA uses, it may be possible to avoid the singularity by evaluating the integral for the nodes (vertices) of the mesh and then interpolating for the face centres. In most cases, however, finer meshes are needed, and the accuracy of this approach is not sufficient.

An alternative method was developed based on a derived analytical expression for the integral value induced by a thin cylindrical slab (like a coin) at the points of its axis. The mesh cells lying immediately below the surface observation point (down to a certain specified depth) are processed in this way, and the contributions of all the other cells are calculated directly with the Biot-Savart formula (43). This approach was observed to give improved results. Problems still exist for neighbouring cells that lie off the normal axis and are still very close to the observation point since no analytical expression is used for their contributions.

Local mesh refinement around the singularity is the third approach that has been investigated. When the contribution of each element of the mesh is being calculated, the ratio between its size and the distance from the element centroid to the observation point is considered. If that ratio is lower than a certain limit (0.35 was found to give sufficient accuracy at a reasonable computational cost) the usual piecewise constant integration is performed, else the element is split into eight (for a hexahedral element) equal volumes, each with their own centroid, and their contributions are evaluated separately. The density of the finite volume mesh depends on the 'skin layer' of the electromagnetic field, and the thickness of the skin layer depends on the frequency and the electrical conductivity.

For the cases of induction heating considered in this work, one-level local mesh refinement was found to perform best of the three methods described.

Another issue with the Biot-Savart integral is the computational cost of its evaluation for large problems. Every cell of the mesh has to be visited for every cell face on the surface at every iteration. Unlike with the differential equations, symmetry cannot be used here to save computation. Clustering the cells into sub-domains can help: for each cluster, depending on the distance to the observation point, either its average values are used or the individual contributions of its cells are calculated. This is straightforward to describe in words but needs careful coding.

#### *4.1.3. Normal current condition*

No electric current can flow out of a conductor into an insulator. Consequently, the normal to the surface components of the electric field vectors $\mathbf{E}_R$ and $\mathbf{E}_I$ must reduce to zero on the conductor surface. On a cell-centred mesh a linear profile can be assumed

$$\frac{\partial E_n}{\partial n} = \frac{0 - E_n}{d_f} = -\frac{1}{d_f}(E_x n_x + E_y n_y + E_z n_z) \tag{44}$$

where $n$ is the direction of the outward to the surface unit normal vector $\mathbf{n}(n_x, n_y, n_z)$, $d_f$ is the distance from the cell centre immediately below the surface to the cell face on the surface, $E_n$ is the local normal component of either of the vectors $\mathbf{E}_R$ and $\mathbf{E}_I$, and $(E_x, E_y, E_z)$ are the solved global components of those vectors, all cell-centre values.

As with (41) and (42), the normal current condition (44) also needs to be transformed from local to global coordinates before it can be used. This can be done by differentiating with respect to $n$ the transformation equations for $E_x$, $E_y$, and $E_z$. The result is in linearised form (31) with the previous iteration values of the other two vector components appearing in the $S_C$ part.

### *4.2. Symmetry and material boundaries*

For the usual symmetry boundary condition the normal derivatives of the solved quantities are set to zero. With **azimuthal symmetry** in a cylindrical geometry the above is quite correct for the scalar variables and the axial components of the vector variables. However, the remaining two vector components need special attention in this case.

In fact, what is required is to make the radial ($E_r$) and the azimuthal ($E_a$) components of a given vector $\mathbf{E}(E_x, E_y, E_z)$ stay constant across the azimuthal symmetry plane, i.e. to ensure

$$\frac{\partial E_r}{\partial \alpha} = 0 \ , \quad \frac{\partial E_a}{\partial \alpha} = 0. \tag{45}$$

where $\alpha$ is the azimuthal angle in cylindrical coordinates. By differentiating with respect to $\alpha$ the transformation expressions $E_r = E_x \cos\alpha + E_y \sin\alpha$ and $E_a = E_y \cos\alpha - E_x \sin\alpha$ it can be shown that the equations

$$\frac{\partial E_x}{\partial \alpha} = -E_y \ , \quad \frac{\partial E_y}{\partial \alpha} = E_x \tag{46}$$

are equivalent to (45). The above relations express the azimuthal symmetry condition in terms of the solved quantities in the global Cartesian coordinate frame. At implementation it would be best to use the outward normal derivatives at the symmetry planes instead of the $\alpha$-derivatives, then $n = \pm r\alpha$ with $r$ being the cylindrical radius of the centre of the given face on the symmetry plane, and the sign depends on which side of the sector domain is being considered. Strictly speaking, expressions (46) use the face values, and on a cell-centred mesh the solved quantities are available at the cell centroids. Assuming linear variation from the centroid to the face centre, new expressions involving only the cell values can be derived. They appear in the form (31) with $S_P = d_f/(r^2 + d_f^2)$ where $d_f$ is the small distance between the cell centroid and the azimuthal symmetry face.

Discontinuities arise at **material boundaries** between two conductors with different electrical conductivity. The principle of charge conservation requires that the normal electric current should be the same either side of any face in the mesh. This means that

$$\sigma_1 E_{1n} = \sigma_2 E_{2n} \tag{47}$$

where $E_{1n}$ and $E_{2n}$ are the face values of the solved electric field vectors in the two materials. If (47) is ignored and the mesh is continuous, the diffusive equations (7) and (8) will smear the jump over several cells across the interface. If that is undesirable, source terms need to be introduced in every pair of cells across the material boundary. Again a transformation from local to global coordinates is needed for the implementation of this boundary condition.

## 5. Validation

It is natural to start testing the numerical procedures with simple cases that are easily verifiable. The **one-dimensional** test with analytical solution (28) and (29) is presented in Figure 1. The 1D computational domain of length 55 mm is divided into 20 mesh cells clustered towards the right end which represents the metal charge surface. This variable mesh spacing allows better resolution within the electromagnetic skin depth ($\delta = 8.5$ mm in this case) without using fine mesh everywhere in the domain. (Such clustering of the mesh becomes especially important in 3-dimensional cases since it leads to significant savings in computational time.) Sinusoidal in time magnetic field is prescribed with amplitude 0.2 T on the charge surface and frequency 7000 Hz. The Biot-Savart integral is not used in this test. Two different numerical results are compared with the exact solution: the result of solving (7) and (8) with boundary conditions (42) is marked "solve E", and the result of solving (26) and (27) with fixed-value boundary conditions is marked "solve B". Excellent agreement is observed with only a minor error where numerical differentiation is used (22) to post-process results.

An **axisymmetric** test case relevant to magnetic levitation has been used to verify a pseudospectral method for modelling induction melting [11]. The test case, which also has an analytical solution, is of the electric current induced in a conducting sphere by a coaxial current ring. The presented results are for frequency 6000 Hz, electrical conductivity of the sphere $4 \times 10^6$ S/m, electromagnetic skin depth $\delta = 3.25$ mm, radius of the sphere 37.5 mm, radius of the single current loop 60 mm and amplitude of the current 1000 A. The finite-volume computational domain covers a $9^o$ wedge (slice) of the sphere with its axis of symmetry being the axis of the current-carrying ring. Azimuthal symmetry boundary conditions, as described in the previous section, are applied on the meridional planes either side of the wedge. The Biot- Savart integral boundary condition is applied on the outer surface of the wedge. When doing this, the remaining 39 spherical sectors which are not in the computational mesh are taken into account by rotating the vectors of the electric current density of the main slice accordingly around the axis of symmetry.

In Figure 2 the electric current density along the radius in the equatorial plane of the sphere is shown at the beginning of a cycle and at a quarter of a cycle. The numerical solution "solve E" was obtained as described above, however, here the magnetic field

on the surface is not known, and it was calculated using (43). It can be seen that the agreement is very good, but it is not perfect. This is due to the accuracy with which the particular implementation of the software handles the singularity of (43).

In the **two-dimensional** case a constant boundary condition (23) may be specified along the surfaces of the conducting bodies which makes this case very useful for test purposes. In Figure 3 results are compared of two separate simulations of a cross-section of an induction-heating device. The external part represents the water-cooled copper 'fingers' of the 'cold crucible' with electrical conductivity $4.1 \times 10^7$ S/m and electromagnetic skin depth 0.94 mm. The internal part (to the left of the drawing) represents the metal charge to be melted which has electrical conductivity 500000 S/m and electromagnetic skin depth 8.5 mm. The driving frequency is 7000 Hz. The upper part of the figure shows the solution of (7) and (8) with a constant value of the magnetic induction ($B_R = 0.1$ T, $B_I = 0$) specified along the surface boundaries. The azimuthal extent of the domain is 30°, and azimuthal symmetry conditions (46) are applied on the artificial boundaries. This result is referred to as "solve E".

The second simulation, "solve B", of the same problem is performed by solving (26) and (27) with the same fixed value of 0.1 T used as surface boundary condition. On the azimuthal boundaries simple no-flux symmetry may be used for the two scalar quantities $B_R$ and $B_I$. The surface conditions are applied to all surfaces, including both sides of the slits in the crucible, with the only exception being the hole in the middle whose walls are approximated as symmetry planes. The electric field is recovered from the solution of the magnetic field using (22) by means of numerical differentiation.

The lower part of Figure 3 presents the difference in the calculated real part of the electric field vector $\mathbf{E}_R$ using methods "solve E" and "solve B" as percentage of the maximum value of the magnitude of $\mathbf{E}_R$ in the domain. The maximum difference is below 2% which is very encouraging.

## 6. Results and Discussion

A *three-dimensional* example is taken from a project on recycling silicon processing waste [12] where the non-conducting crucible often has square cross-section (Figure 4).

The meshed computational domain covers 1/4 of the volume of molten silicon inside the crucible with $y = 0$ and $x = 0$ being symmetry planes. The side of the square cross-section is 35.4 mm and the height of the melt volume is 65 mm. The external coil is represented as 10 rings of electrical current lines with radius 47 mm spaced vertically at 17 mm from each other with the lowest turn located 50 mm below the lower end of the meshed volume. The amplitude of the coil current is 544.5 A and its frequency is 3000 Hz. The electromagnetic skin depth in this case is 8.3 mm.

The 3-dimensional calculation according to (7), (8), (9) and (10) shows the amplitude of the vertical $z$-component of the magnetic induction on the inner crucible wall (the outer surface of the meshed volume) is around 38 mT on average (Figure 5). For comparison, this value was prescribed as the boundary condition of the "solveB" 2-dimensional implementation based on (26) and (27) in a square domain with the same side length as the 3D one. As it can be seen in Figure 6 and 7, the resulting electromagnetic field, force field and heat sources are quite similar. Both comparisons are between values at height 1/3 from the top of the domain in the 3D case "solve E" and the corresponding 2D results "solve B".

The similar cross-section values are expected as the electromagnetic field has nearly 2-dimensional structure at the chosen height. However, near the top and the bottom of the domain, significant deviation from the from the 2D pattern is observed (Figures 4 and 5) which justifies the need for 3D modelling capability.

## 7. Conclusions

The finite volume method has been applied to the solution of the equations of electromagnetic induction. Primitive variables have been used rather than a magnetic vector potential. Only the charge of the induction furnace (the conducting body or liquid where eddy currents are induced) is included in the meshed computational domain, and the influence of the driving coil current is accounted for by means of integral equations. In this way the same mesh can be used simultaneously for all aspects of the modelled physics: electromagnetism, fluid flow, turbulence, heat transfer, etc. This common mesh would also be very useful in true magnetohydrodynamic cases where the induction and the flow

are closely coupled (inter-dependent on each other).

In *two-dimensional* quasi-steady simulations for the cross-sections of induction furnaces, selecting the real and imaginary part of the *magnetic induction* as solved variables is the most accurate and computationally efficient approach. This option needs an estimate of the magnetic field strength between the coil and the charge to be prescribed as boundary condition (and the solution re-iterated if necessary). Solving for the *electric field* vector and for an additional scalar potential (real and imaginary parts) is a generic option for *3-dimensional* quasi-steady models. This full model does require calculation of the magnetic field integral for all cell faces on the surface of the charge which may lead to longer computational times but a clustering approach to the implementation of the integral evaluation (where cells further away from the observation point are clustered together and only their average is used in the calculation) helps reducing the run time even without parallel computation.

Extensive validation of the new 3-dimensional method was accomplished by comparing with (a) 1D theoretical results, (b) 2D cross-section results and (c) 2D axisymmetric analytical results in a vertical plane perpendicular to the cross-sectioning plane. A fully 3-dimensional example shows the applicability of the method to real industrial problems, in this case - the electromagnetic field in a volume of silicon remelted in a crucible with a square cross-section with the aim of purifying it and reusing it in photo-voltaic cells.

The procedures described in this paper provide a method for modelling the operation of induction furnaces, as well as closely coupled magnetohydrodynamic phenomena in complex geometries. They are most useful in cases of visible penetration of the magnetic field into the heated charge, e.g. more than 2% of the radius or equivalent size parameter. The smaller the electromagnetic skin depth, the more clustered towards the surface of the charge the computational mesh needs to be in order to achieve adequate resolution. For even higher frequencies when the mesh at the surface would become impractically fine, there is no need to solve numerically the PDEs of the electromagnetic field; instead, the 1-dimensional analytical result (28, 29) can be integrated over a chosen suitable depth and the resulting force and heat applied as source terms in the corresponding fluid and thermal PDEs.

**Acknowledgments**

This work was financed through two separate research projects: (1) Grant GR/N14316/01 by EPSRC (Net-shape casting of TiAl components) and (2) SIKELOR[12] - a project funded by the 7th Framework Programme of the European Commission, subprogramme: ENV.2013.6.3-1, project reference 603718.

**References**

**References**

[1] S. L. Ho, Y. Li, X. Lin, E. W. C. Lo, K. W. E. Cheng, K. F. Wong, Calculations of eddy current, fluid, and thermal fields in an air insulated bus duct system, IEEE Transactions on Magnetics 43 (4) (2007) 1433–1436.

[2] F. Bay, V. Labbe, Y. Favennec, J. Chenot, A numerical model for induction heating processes coupling electromagnetism and thermomechanics, Int. J. Numer. Meth. Engng 58 (2003) 839–867. doi:10.1002/nme.796.

[3] N. Croft, K. Pericleous, M. Cross, PHYSICA: A multiphysics environment for complex flow processes, in: C. Taylor, et al. (Eds.), Numerical Methods in Laminar and Turbulent Flow, Vol. 9, part 2, Pineridge Press, U. K., 1995, pp. 1269–1280.
URL http://staffweb.cms.gre.ac.uk/~physica

[4] A. Kalimov, S. Vaznov, T. Voronina, Eddy current calculation using finite element method with boundary conditions of integral type, IEEE Transactions on Magnetics 33 (2) (1997) 1326–1329. doi:10.1109/20.582500.

[5] Q. Chen, A. Konrad, P. Biringer, A Finite Element - Green's Function method for the solution of unbounded three-dimensional eddy current problems, IEEE Transactions on Magnetics 30 (5) (1994) 3048–3051. doi:10.1109/20.312580.

[6] J. Ruan, X. Chen, K. Zhou, Z. Ren, 3D transient eddy current calculation by the hybrid FE-BE method using magnetic field intensity H, IEEE Transactions on Magnetics 31 (3) (1995) 1408–1411. doi:10.1109/20.376291.

[7] E. Haber, U. Ascher, D. Aruliah, D. Oldenburg, Fast simulation of 3d electromagnetic problems using potentials, Journal of Computational Physics 163 (2000) 150–171. doi:10.1006/jcph.2000.6545.

[8] F. Matsuoka, A. Kameari, Calculation of three-dimensional eddy current by FEM-BEM coupling method, IEEE Transactions on Magnetics 24 (1) (1988) 183–185.

[9] R. Moreau, Magnetohydrodynamics, Kluwer Academic Publishers, 1990.

[10] S. V. Patankar, Numerical Heat Transfer and Fluid Flow, Hemishere Publishing Co., 1980.

[11] V. Bojarevics, K. Pericleous, M. Cross, Modeling the dynamics of magnetic semile-vitation melting, Metallurgical and Materials Transactions B 31B (2000) 179–189.

[12] SiKELOR, http://cordis.europa.eu/project/rcn/110318_en.html, http://www.sikelor.eu, accessed: 28 Oct (2014).

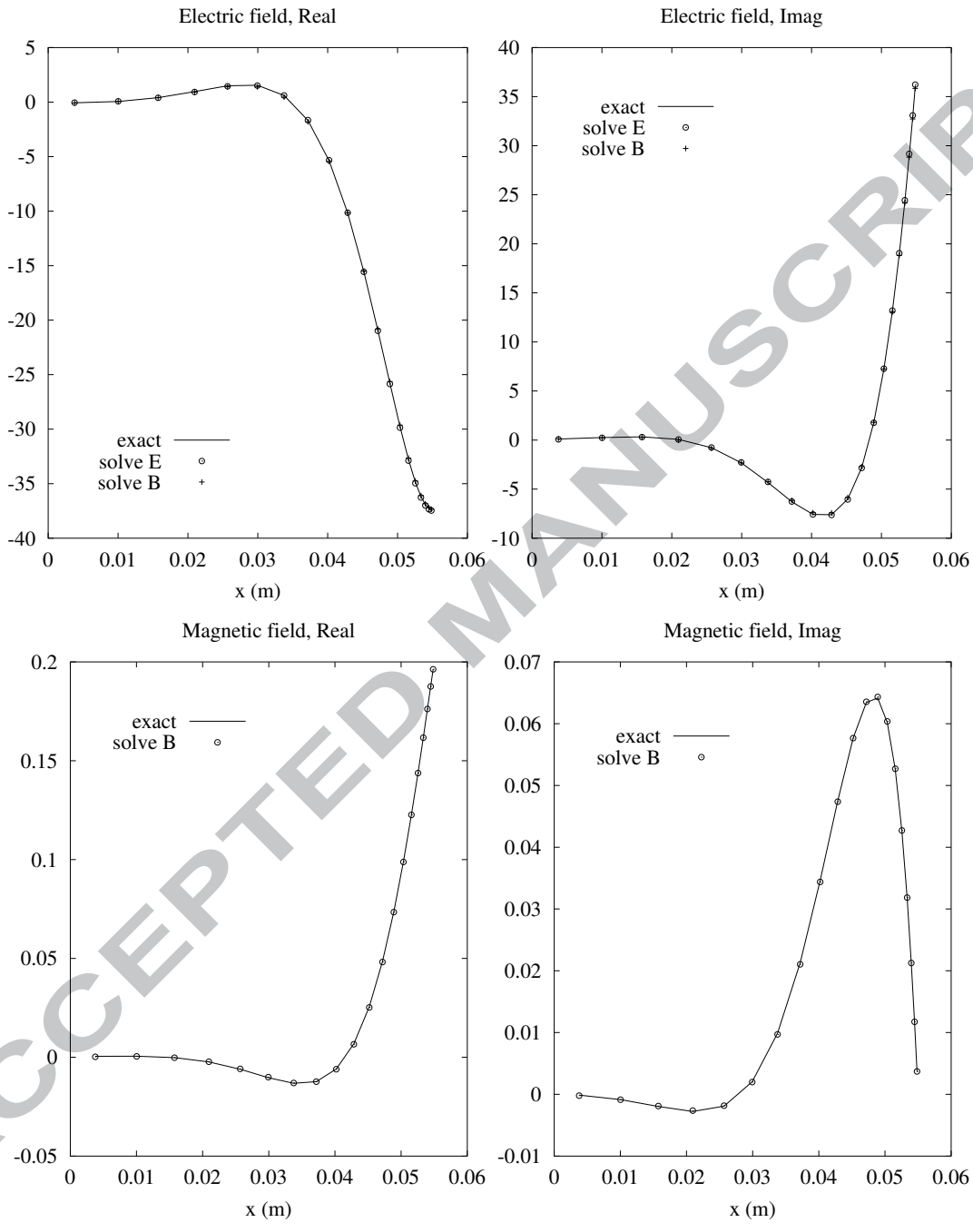


Figure 1: Validation results for 1D test problem

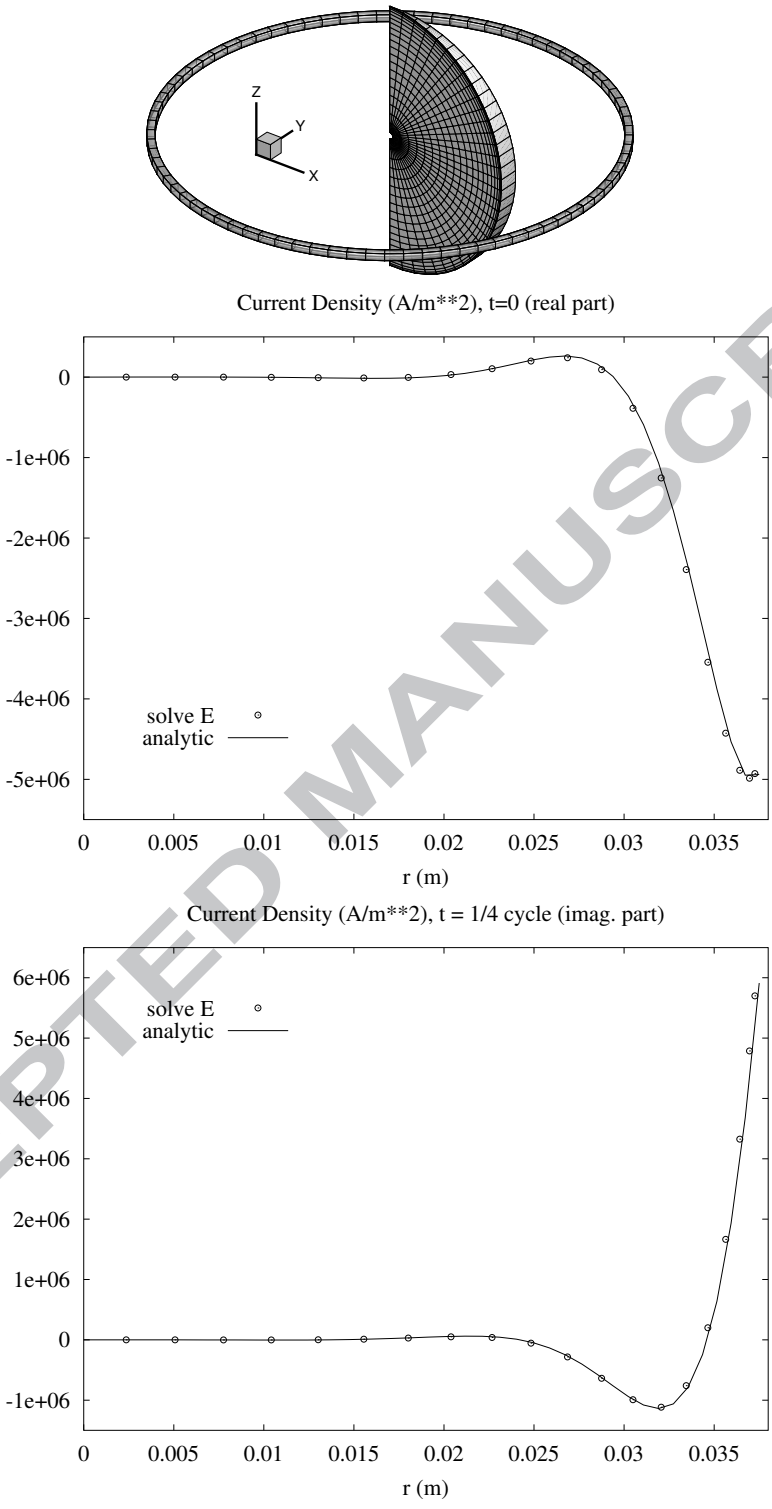


Figure 2: Axisymmetric solution for test sphere: computational 'wedge' domain, current loop and results on equatorial plane

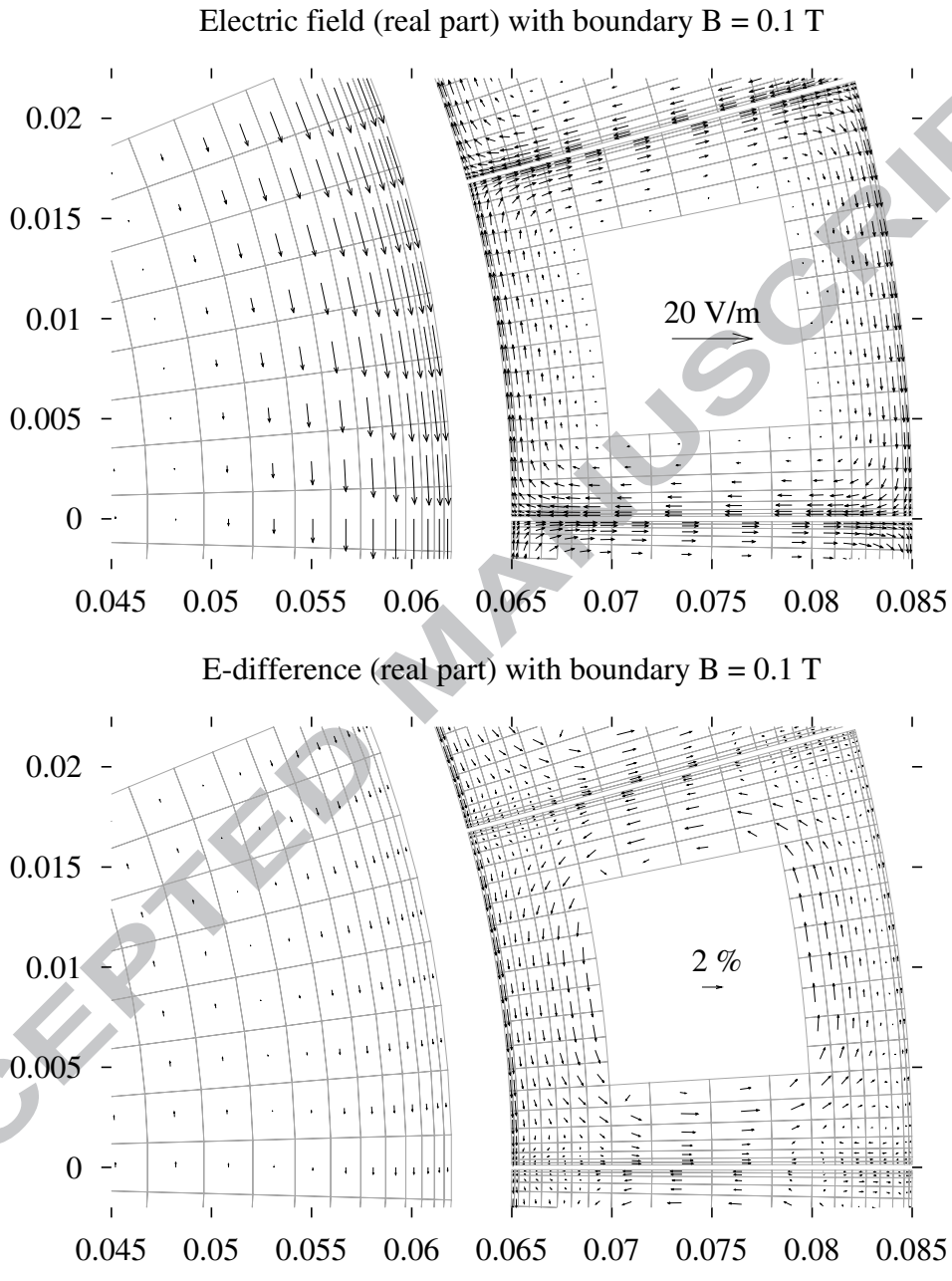


Figure 3: 2D test (horizontal section of 'cold-crucible' induction furnace): above - solved electric field; below - difference between "solve E" and "solve B"

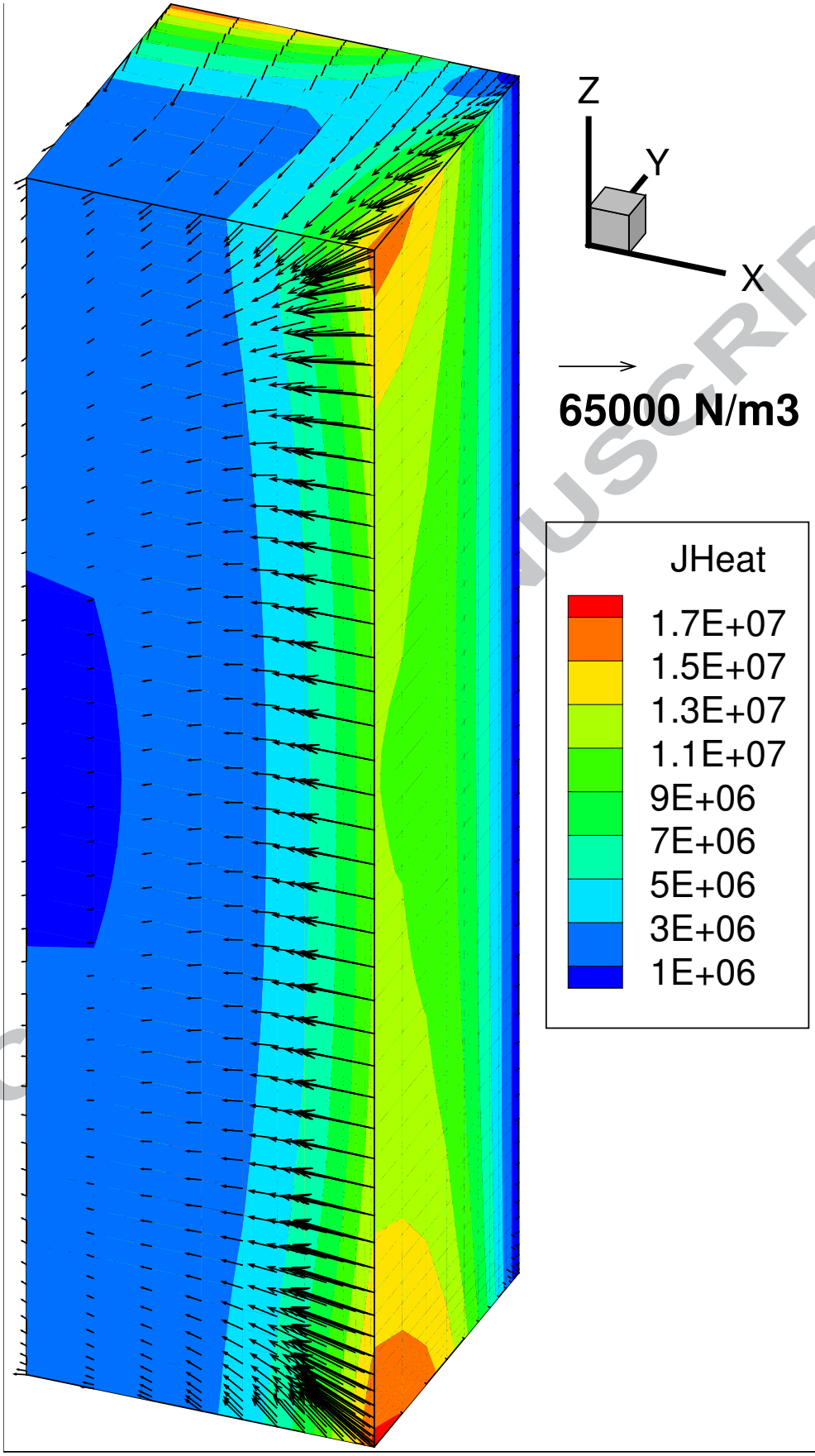


Figure 4: Joule heat source (contours) and Lorentz force (vectors) in a quarter of experimental Si melt in a square crucible

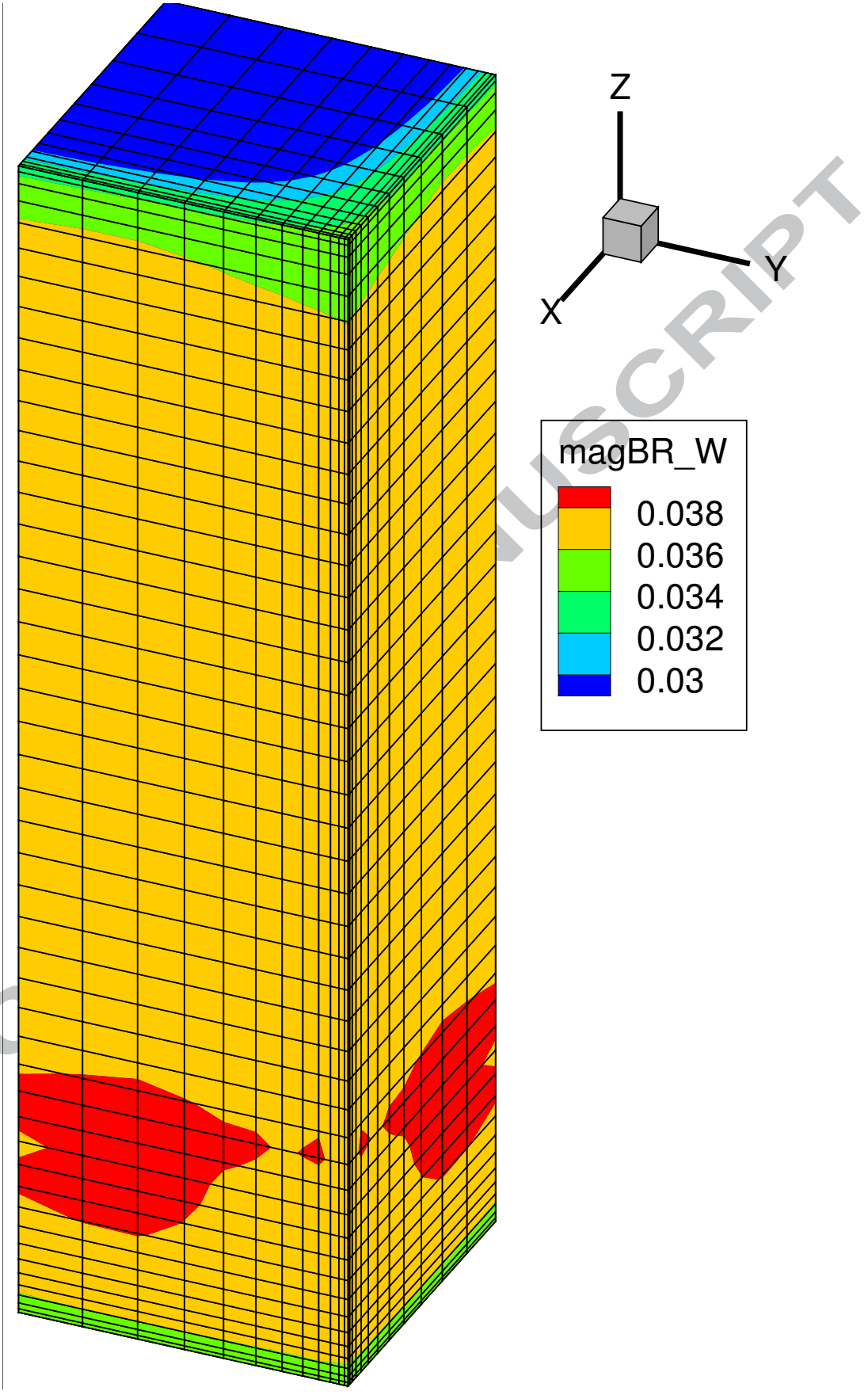


Figure 5: Vertical component of the computed 3D magnetic field

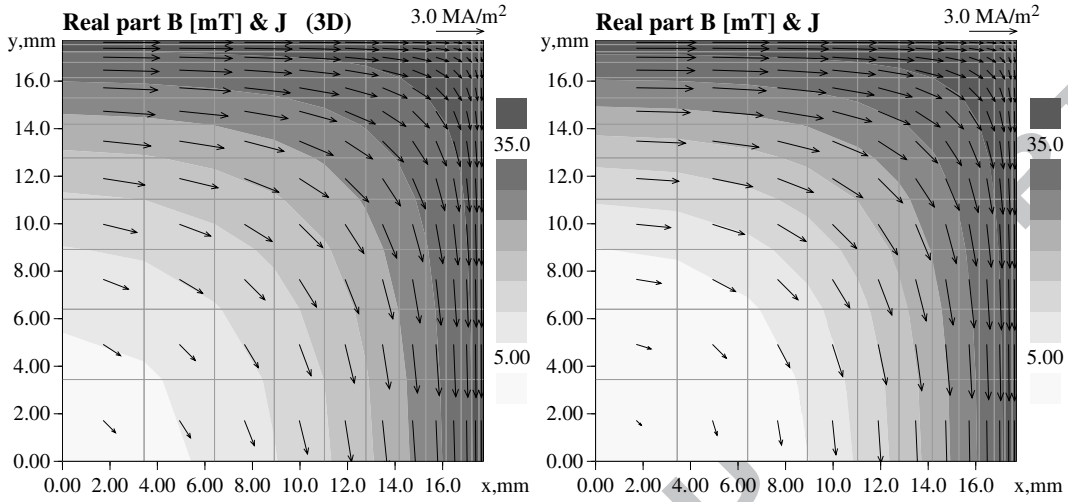


Figure 6: Comparison of "solve E" (left) and "solve B" (right) electromagnetic field

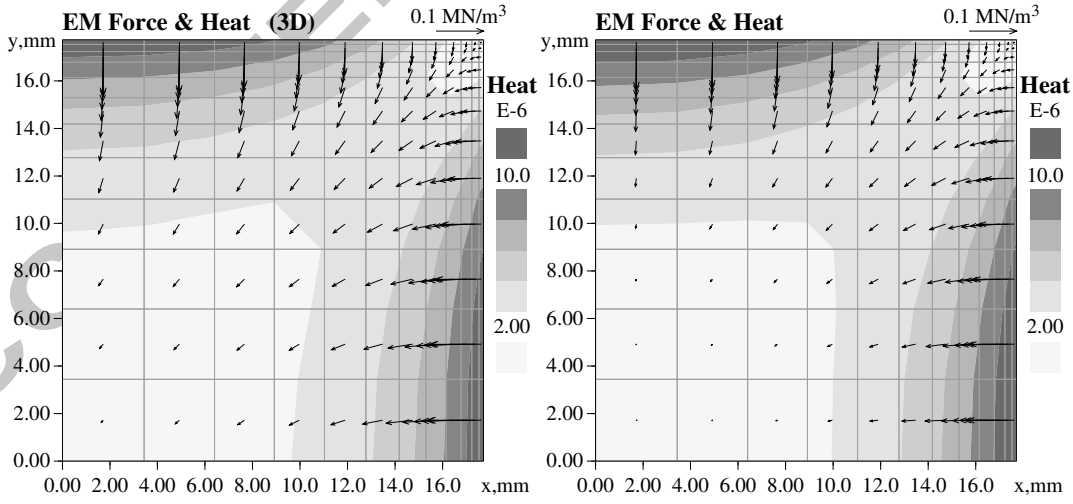


Figure 7: Comparison of "solve E" (left) and "solve B" (right) Joule heating and electromagnetic (Lorentz) force field